



The influence of glacial topography on fluvial efficiency in the Teton Range, Wyoming (USA)



Sarah E. Johnson ^{a,*}, Meredith L. Swallom ^a, Ryan Thigpen ^a, Michael McGlue ^a, Jason M. Dortch ^b, Sean Gallen ^c, Edward Woolery ^a, Kevin M. Yeager ^a

^a Department of Earth and Environmental Sciences, University of Kentucky, Lexington, KY 40506, USA

^b Kentucky Geological Survey, University of Kentucky, Lexington, KY 40506, USA

^c Department of Geosciences, Colorado State University, Fort Collins, CO 80523, USA

ARTICLE INFO

Article history:

Received 29 November 2021

Received in revised form 15 May 2022

Accepted 24 May 2022

Available online xxxx

Editor: J.P. Avouac

Keywords:

post-glacial fluvial erosion

Teton Range

denudation

landscape evolution

sediment budget

erosion rates

ABSTRACT

This study examines the role of **topography as a dynamic boundary condition** that limits the efficiency of fluvial erosion in the post-glacial Teton Range landscape. The volume of sediment currently stored in two major catchments was estimated using high-resolution LiDAR and geometric reconstructions of depth to bedrock. Seismic reflection data in Moran Bay reveals post-glacial sediment preserved behind a submerged moraine, which isolates the bay from the larger Jackson Lake depocenter. The volume of post-glacial sediment stored in the canyons and bay totals $173.82 \pm 19.5336 (\times 10^{-3} \text{ km}^3)$, which translates to a catchment-wide sediment production rate of $0.17 \pm 0.02 \text{ mm/yr}$. The rock-equivalent sediment volume in Moran Bay is $4.4 \pm 0.9 (\times 10^{-3} \text{ km}^3)$, only $\sim 2.6\%$ of the total post-glacial volume. While the estimated sediment production rate in the canyons is similar to the uplift rate, the denudation rate derived from Moran Bay sediment is $0.004 \pm 0.001 \text{ mm/yr}$, implying highly inefficient post-glacial sediment transport. The fluvial system has been disequilibrated by glacial erosion such that interglacial valley profiles lack the steepness needed to transport sediment, delaying sediment evacuation until the next glacial advance, or until uplift sufficiently steepens the fluvial system so that it regains efficiency. Furthermore, colluvial production rates in the deglaciated valleys are close to long-term denudation and uplift rates, suggesting that once topography has been equilibrated to glacial erosion processes, subsequent glaciers do not need to produce much bedrock erosion, but mainly sweep out accumulated sediment to maintain equilibrium.

© 2022 Elsevier B.V. All rights reserved.

1. Introduction

The relationships and feedbacks between rock uplift, denudation and topography remain enigmatic, and many studies regard topography as merely a record of the interplay between tectonic and climatic forces. The role of climate in driving fluvial and glacial processes that keep pace with (or enhance) rock uplift has been thoroughly examined (Mitchell and Montgomery, 2006; Egholm et al., 2009; Koppes and Montgomery, 2009; Whipple, 2009; Binnie and Summerfield, 2013; Adams et al., 2020; Spotila, 2022) although a definitive consensus remains elusive. The potential role of topography itself as a dynamic boundary condition that controls the rate of denudation and sediment transport has received far less attention. This study examines how topography limits the efficiency of fluvial erosion, thus imposing a threshold that

must be overcome for the fluvial system to effectively respond to uplift. As glaciers retreat, a paraglacial landscape with oversteepened valley walls produces sediment rapidly (Norton et al., 2010; Ballantyne, 2013). However, deglaciated valley bottoms typically lack the profile steepness to facilitate fluvial erosion and sediment evacuation (Dortch et al., 2011; Moon et al., 2011). Thus, if the glacial topographic conditioning is exhaustive, topography itself creates a protracted lag in fluvial response time, similar to moraine dams preventing fluvial incision in high mountains (e.g., Korup and Montgomery, 2008). The impacts of continued climate change and glacial ablation may lead to development of numerous inefficient rivers, which can impact sediment transport and water supply (Herman et al., 2021).

Although sediment volumes or production rates have been estimated for deglaciated valleys in a number of locations (e.g., Otto et al., 2009; Tunnicliffe and Church, 2011; Tranel et al., 2015; Ardelean et al., 2017), documentation of complete post-glacial catchment sediment budgets from source to sink is rare (e.g., Fame et al., 2018). Studies of fluvial transport in deglaciated catchments

* Corresponding author.

E-mail address: Sarah.Johnson11@uky.edu (S.E. Johnson).

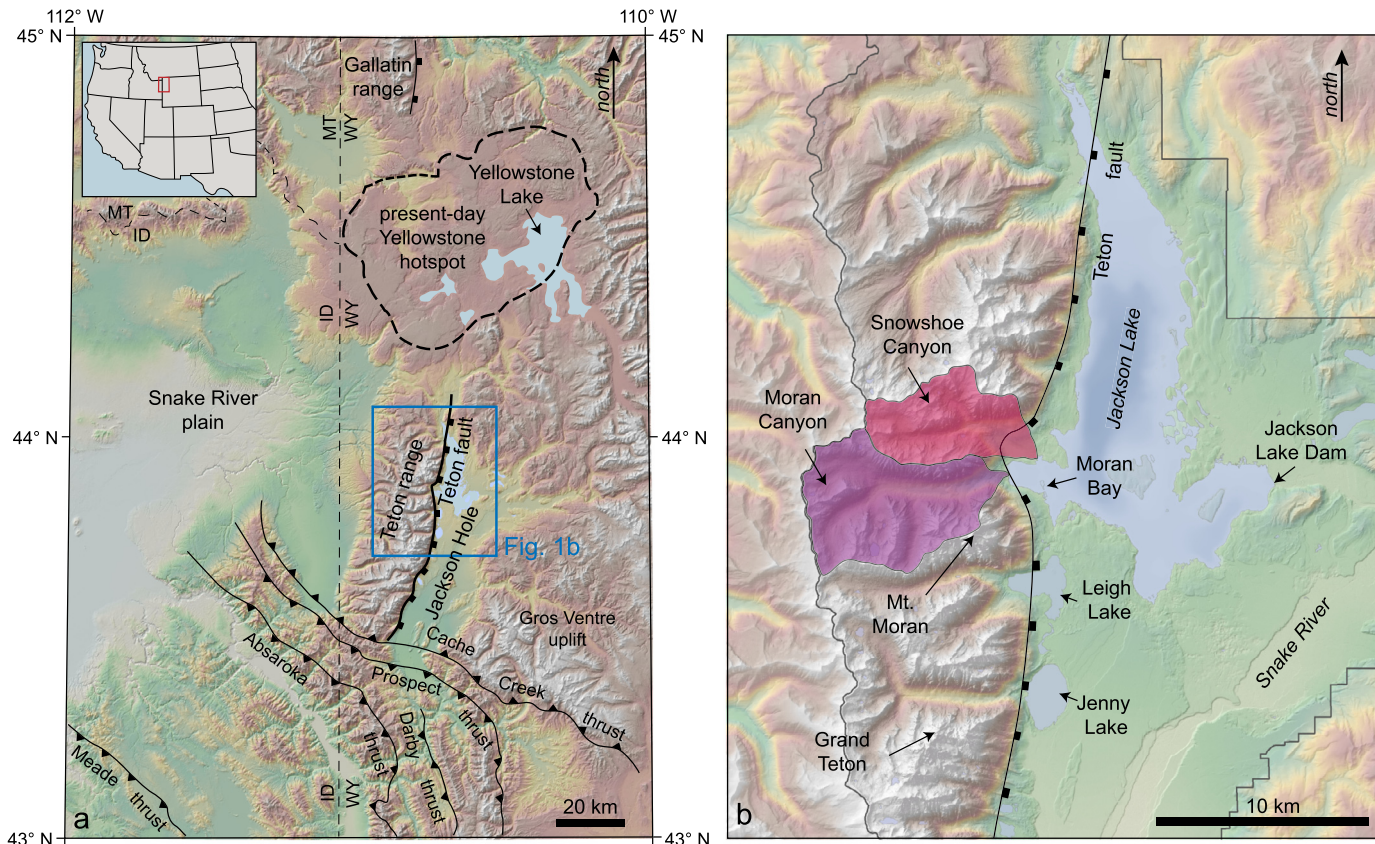


Fig. 1. a) Regional map of the Teton Range which lies at the eastern edge of the Basin and Range in northwestern Wyoming. Displacement along the Teton normal fault that bounds the eastern side of the range has produced an asymmetric uplift that dips to the west. b) Moran and Snowshoe Canyons drain into Moran Bay, the westernmost portion of Jackson Lake. The terminal moraine formed by the Pinedale glacial advance (14.4 ± 0.8 ka) impounded Jackson Lake.

have focused on enhanced sedimentation in lower reaches where fluvial processes dominate (Church and Ryder, 1972; Ballantyne, 2013), in contrast to the upper paraglacial reaches where glacial drift is less abundant and rivers are smaller (Dietsch et al., 2015). Field-based denudation studies often rely on the assumption that short-term (days to years) observations of suspended sediment yields from modern rivers represent long-term (10^4 – 10^6 years) denudation rates, yet these rates can be quite variable through time (Koppes and Montgomery, 2009; Spotila, 2022). Various strategies have also been employed to model fluvial erosion, but there are few studies that directly quantify mass flux (Adams et al., 2020). These knowledge gaps lead to uncertainty in the governing relationships between uplift, denudation and topography, leading to a reliance on modeling for insight (Pedersen and Egholm, 2013).

To assess fluvial efficiency in a relict glacial landscape and address spatial-temporal data disparities, a complete post-glacial sediment budget and long-term (10^4 – 10^8 years) uplift and denudation data are necessary. The Teton Range (Wyoming, western USA, Fig. 1) provides an ideal natural setting to examine this problem, as fluvial sediment derived from two deglaciated catchments is trapped in a perched lacustrine basin (Moran Bay), thus allowing a post-glacial sediment budget to be constructed. Existing high-resolution light detection and ranging (LiDAR) topographic data allows detailed geomorphologic mapping of glacial and post-glacial sediment and the estimation of sediment volumes and production rates. Seismic reflection data acquired for this study in Moran Bay reveals a complete post-glacial (14.4 ka) sediment package from two major catchments in the range, from which sediment volumes can be estimated. The glacial history has been constrained by ^{10}Be cosmogenic dating of glacial moraines (Pierce et al., 2018), and the uplift history is well-constrained by multiple low-T thermochronol-

ogy studies (Brown et al., 2017; Thigpen et al., 2021). Here, we leverage these datasets to quantify post-glacial sediment production and flux from source to sink. We find that although hillslope sediment production rates are close to uplift rates, glacially carved valley bottom gradients limit efficient fluvial sediment flux, stalling sediment evacuation until the next glacial advance, or until uplift sufficiently steepens the system to again become efficient.

1.1. Geologic setting

The Teton Range lies at the eastern edge of the Basin and Range in northwestern Wyoming (Fig. 1). Normal displacement along the Teton fault on the eastern edge of the range has produced a west-dipping asymmetric uplift (Foster et al., 2010; Brown et al., 2017). Precambrian units in the range center are unconformably overlain by west-dipping Paleozoic and Mesozoic strata (Love et al., 1992). The onset of Teton fault slip is ~ 10 Ma, and displacement estimates range from 11.4–12.6 km (Thigpen et al., 2021). Although the Teton Range lies within the Intermountain Seismic Belt, the Teton fault remains quiescent, with no evidence of a major slip event in the past 5 ka (DuRoss et al., 2019).

Multiple glacial advances during the Quaternary carved the spectacular Teton relief (>2 km, Good and Pierce, 2016) and has driven range divide migration to the west (Foster et al., 2010; Zhu et al., 2021). Evidence from the most recent Bull Lake (170–130 ka) and Pinedale (20–12 ka) glaciations indicate that the Yellowstone ice cap extended into the Jackson Hole valley, and alpine glaciers in the Teton Range flowed east to join the main glacial lobe (Pierce et al., 2018). The Pinedale advance formed the terminal moraine, which naturally impounded Jackson Lake and the multiple moraine lakes on the range front. Completion of the Jackson Lake dam in

1916 raised the natural lake level by ~12 m. Moran and Snowshoe Canyon, two major Teton catchments, both drain into Moran Bay in the western part of Jackson Lake (Fig. 1). They are similar to other Teton catchments that have drainage areas of >20 km², and their topographic signature is typical of glaciated topography, with deeply incised canyons and elongated and flattened valley profiles (Whipple et al., 1999). Modern wind and precipitation patterns are similar to those from the last glacial maximum (LGM) while pollen studies indicate that vegetation changed from alpine meadow to mixed pine-spruce-fir forest following deglaciation (Whitlock, 1993; Foster et al., 2010).

2. Methods

2.1. Moran Bay seismic acquisition and sediment volume estimate

Stratigraphic horizons bounding the sediment package in Moran Bay were mapped using a grid of CHIRP seismic profiles, acquired using an Edgetech SB-0512i CHIRP sub-bottom profiler. Data were acquired at a tow velocity of ~3 knots and shot points were collected at 2 s intervals across a frequency range of 0.4–4.0 kHz. Seismic data were processed in Seisware using a bandpass filter and amplitude gain. Time-depth conversions were calculated using a constant velocity of 1500 m/s, as unconsolidated sediment is in hydrostatic equilibrium with freshwater (Kindinger et al., 1994). Sediment volumes between mapped stratigraphic horizons were calculated using Trinity T3 software.

2.2. Geomorphologic map

Landforms in Moran and Snowshoe Canyons were mapped using a combination of digital terrain analysis and photo interpretation (Otto et al., 2009; Ardelean et al., 2017). Maps were produced in GIS software using a 0.5 m digital elevation model (DEM) and derivative maps produced from airborne LiDAR (National Park Service, 2014) and 0.3 m Google Earth® satellite imagery from 2013 and 2015. Moran Canyon landform interpretations were field-checked in 2021. Mapped geomorphologic units include talus cones, debris fans, talus slopes, alluvium, glacial drift, moraines, rock glaciers, and bedrock.

2.3. Canyon sediment volume estimates derived from modeled bedrock DEM

The bulk sediment volume in the main trunk of Moran Canyon and two tributary canyons was estimated by differencing a LiDAR-based surface DEM and a modeled bedrock DEM. Because glacial drift is not observed to be deposited upon or interfingering with older colluvial or alluvial deposits, we interpret that pre- and syn-Pinedale (14.4 ± 0.8 ka) colluvial and alluvial deposits were evacuated from the canyon during that glacial period. If correct, mapped colluvial and alluvial deposits should have been derived from the current interglacial period. In sediment volume estimates, it is assumed that mapped boundaries of deposits extend vertically down to bedrock, though it is acknowledged that there may be underlying glacial debris.

Cross sections of the bedrock surface beneath the canyon floor sediment were projected along 33 lines using exposures of bedrock on either side of the canyon; 12 of these cross-sections are also constrained by limited canyon floor bedrock exposures (Fig. 2a), which were confirmed via field checking. Prominent irregularities in the bedrock surface DEM were smoothed using the focal statistics tool in ArcGIS with a circular radius of 10 m and then sampled every 10 m to generate the cross sections. A smoothing spline function within the MATLAB curve-fitting toolbox was used to project a bedrock surface beneath the surface for each cross

section; smoothing spline values ranged between 0.94 and 0.99. The smoothing spline function fits a curve piecewise to each data point; the value ranges from 0, where it produces a least-squares straight-line fit, to 1, where it produces a cubic spline interpolant. This method prevents overestimation of bedrock depth that can be produced by a polynomial function (Fig. 2b). The final bedrock surface DEM was generated from the projected bedrock cross sections and supplementary points in ArcGIS using the Topo to Raster tool, which uses an iterative finite difference interpolation technique. Supplementary points were added along valley walls at the contacts of colluvium and exposed bedrock, at exposed bedrock in the valley bottom, and in other locations where the modeled DEM appeared to either over-estimate sediment depth or rise above the ground surface (Fig. 2b). This methodology is similar to Schrott et al. (2003), although that study used polynomial functions that led to an overestimation of bedrock depth, particularly when valleys were relatively narrow. Tranell et al. (2015) used exposed bedrock slopes above talus cones in the Tetons to project the bedrock below the talus and estimate individual talus cone volumes, which produced values similar to those presented here. Lastly, we conservatively incorporate a ±20% uncertainty for estimates of the total sediment volume and denudation rates in the canyons.

2.4. Canyon sediment volume estimates derived from colluvial sediment production rate

The bulk volume of talus cones and debris fans was divided by their contributing source area to calculate a catchment-averaged colluvial production rate. Outside of the modeled bedrock DEM area, the colluvial production rate was applied to source areas of talus cones and debris fans to estimate their bulk volume.

2.5. Canyon sediment volume estimates derived from assigned thickness

To estimate sediment volumes for areas where there are talus slopes, rock glaciers, small cirque moraines, lakes, and areas of glacial drift, sediment thicknesses were assigned based on geospatial data and field observations. To account for uncertainties associated with these estimates, total rock volume calculations and denudation rates are reported with and without these values.

Outside of the area covered by the bedrock DEM, glacial drift is assigned a thickness of 2.4 ± 1.3 m based on the average of 65 gully depth observations. The bulk volumes of cirque moraines and rock glaciers were individually estimated by measuring their heights over the surrounding terrain and multiplying by their mapped area. The average thickness of the nine cirque moraines and eight rock glaciers is 8.1 ± 3.6 m and 12.3 ± 6.7 m, respectively. We have estimates of the average thickness of talus slopes and alluvium from the modeled bedrock DEM area, but to avoid overestimation, we reduce these average thicknesses in areas outside of the modeled bedrock DEM area. While talus slopes average 6.9 m thick in the modeled DEM area, for areas outside of this, we assign an average thickness of 3.0 m. The average estimated thickness of alluvium in the main trunk of Moran Canyon is 14.3 m in the modeled bedrock DEM area. Other deposits of alluvium occupy smaller areas, and so to avoid overestimation are assigned an average thickness of 5.0 m. Sixteen small lakes in the canyons have formed upon areas of bedrock, talus, drift, and alluvium and were assigned a nominal thickness of 1.0 m.

2.6. Porosity estimates

For each material, porosity estimates are required to convert bulk sediment volumes to solid rock volumes. Although talus porosity is generally heterogeneous, previous studies, including studies in the Tetons, calculated a narrow range (0.20–0.26) of

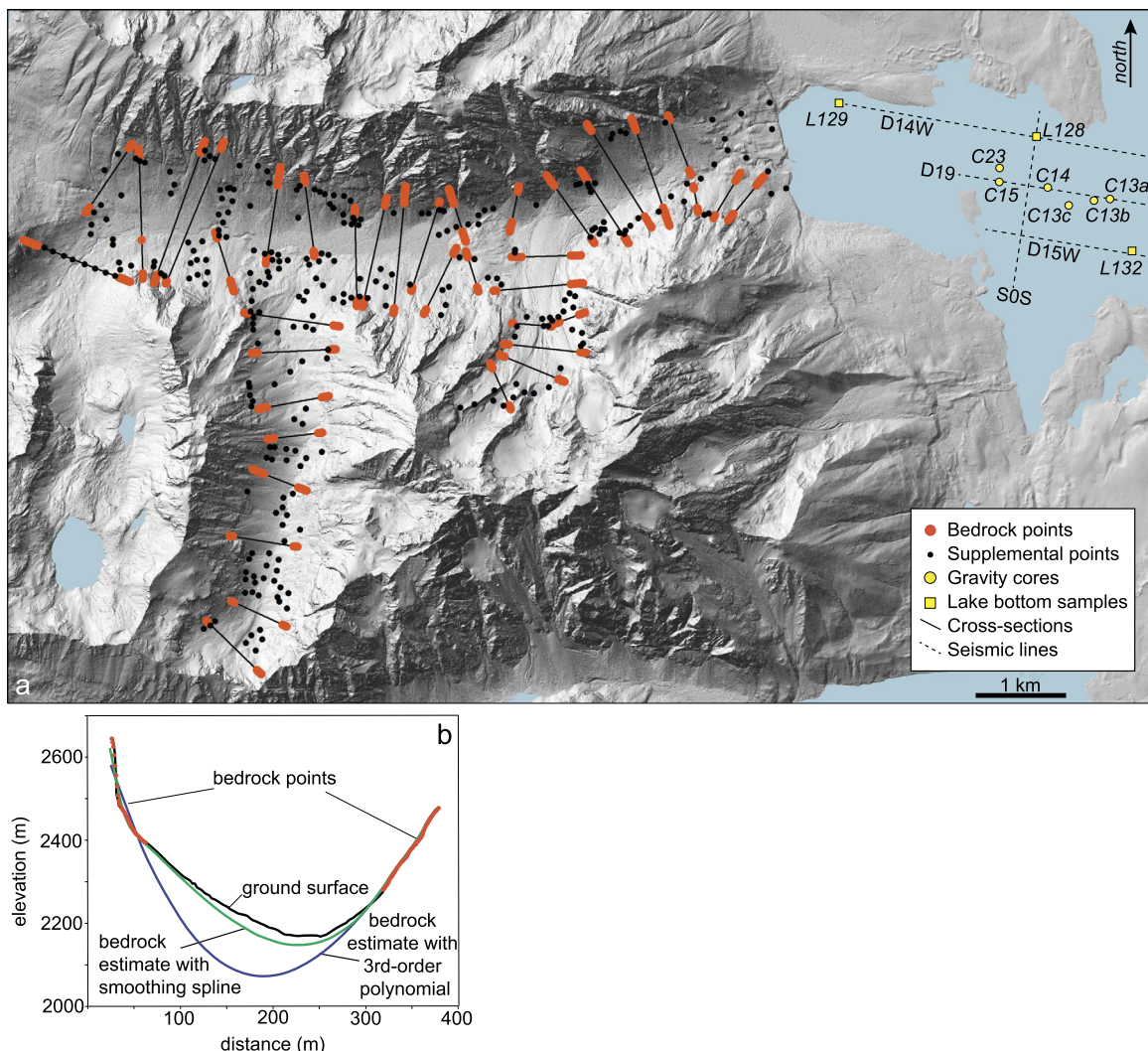


Fig. 2. a) Thirty-three cross sections in the Moran catchment were used to project the bedrock surface under the sediment. Four CHIRP seismic profiles (D19, D14W, D15W and SOS) were used to estimate the volume of sediment derived from the Moran and Snowshoe catchments, and lake bottom samples and gravity cores were used to support the seismic interpretation. b) Example of bedrock surface produced in MATLAB using elevations of exposed bedrock along the valley walls to project the bedrock surface under the sediment.

talus porosity (Tranel et al., 2015; Otto et al., 2009; Sass and Wollny, 2001). Alluvium and glacial drift porosities span large ranges of 0.06 to 0.48 (Frings et al., 2011) and 0.01 to 0.43 (Kilfeather and van der Meer, 2008), respectively. For rock glaciers, a porosity range of 0.40 to 0.60 (Hauck et al., 2011) was used. A porosity range of 0.35–0.45 was used for Moran Bay sediments, based on porosity estimates of Moran Bay short cores and typical values for clay, silt and sand (Leopold et al., 1964).

2.7. Monte Carlo simulation for rock volume and erosion rate calculations

A Monte Carlo simulation with 50,000 iterations was performed to calculate rock volumes and denudation rates. We assumed a normal distribution of values for the bulk sediment volume, post-glacial time, and porosities. We built in uncertainty for the bulk sediment volume by incorporating $\pm 20\%$ range for the volume estimates, and a post-glacial time of 14.4 ± 0.8 ka. The range of porosity values includes standard deviations calculated using the range rule (range $\div 4$). An extreme minimum value for the volume of stored canyon sediment was also calculated by omitting volumes derived from assigned thicknesses. The post-glacial sediment production rate was calculated by dividing the post-glacial

rock volume in the canyons and bay by the catchment area and the post-glacial deposition time interval; the post-glacial fluvial erosion rate was calculated by dividing the rock volume in the bay by the catchment area and post-glacial time.

3. Results

3.1. Geomorphologic mapping of Moran and Snowshoe Canyons

The geomorphologic units in Moran and Snowshoe Canyons (Fig. 3) include talus cones, debris fans, glacial drift, alluvium, talus slopes, rock glaciers and cirque moraines (Fig. 4). In the canyons, talus cones and debris fans dominate the landscape. Talus cones have linear slopes of $\sim 25^\circ$ and range in height from 50–400 m. Debris fans have gently concave slopes averaging $\sim 17^\circ$, often have obvious debris flow tracks, and are up to 200 m high. Glacial drift deposits, present at higher elevations, are generally vegetated, include scattered boulders, and have either a network of gullies or are knobby with intermittent exposures of bedrock. Slopes with talus and periglacial debris are grouped together as talus slopes. Rock glaciers, which are distinguished by their interior arcuate lobes, reach lengths as long as 1.2 km and rise up to 25 m above the surrounding terrain. Some small moraines in the upper basins

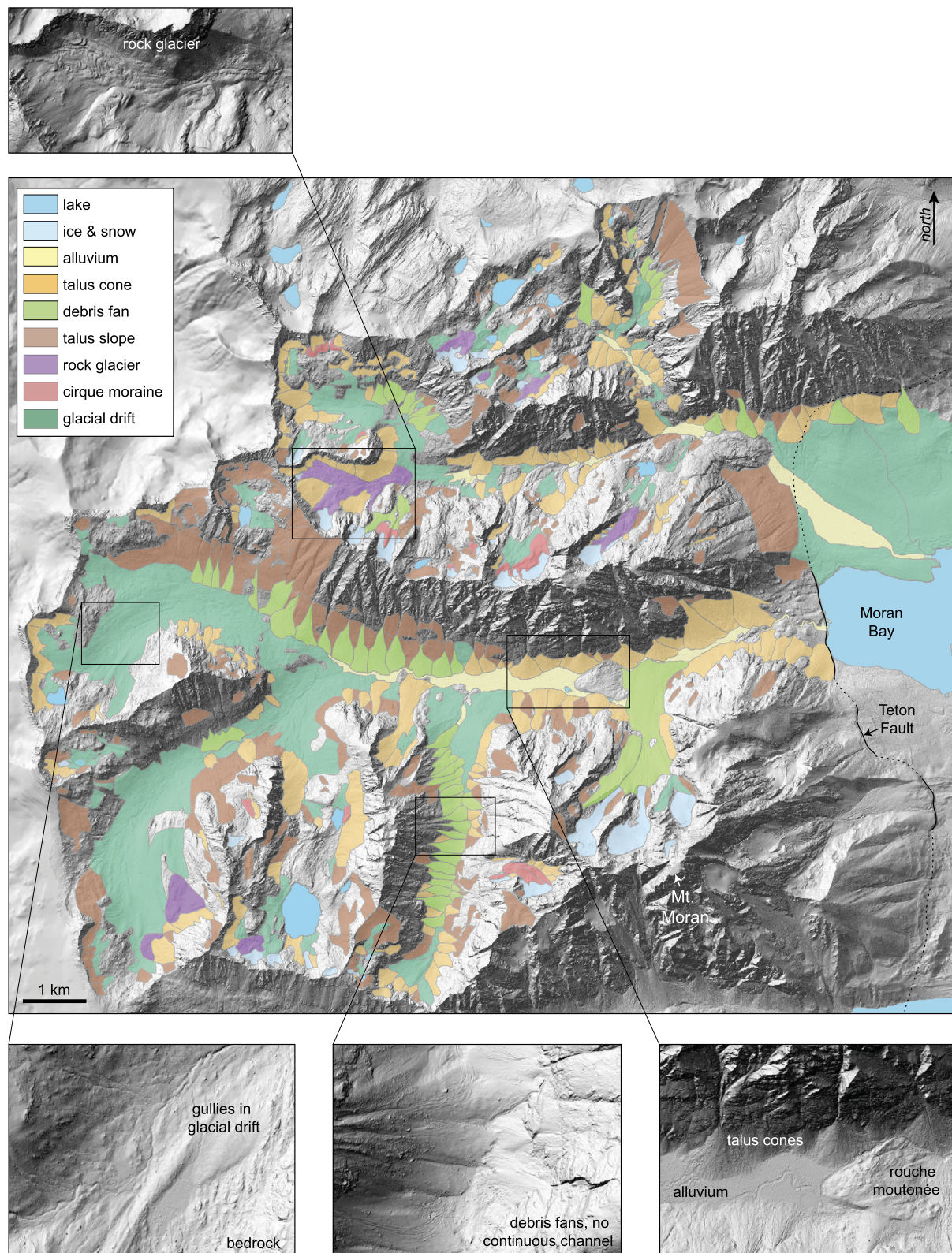


Fig. 3. Geomorphologic map of the Moran and Snowshoe catchments. The base map is a hillshade map derived from LiDAR flown in 2014. Callouts show examples of talus cones, debris fans, alluvium, glacial drift, a rock glacier, and a roche moutonnée.

have crests up to 20 m above the surrounding terrain. Alluvial deposits are distinguished by their flat topography, which is cut by sinuous stream channels and meander scars.

The 6.6 km-long main trunk of the 44.4 km² Moran catchment is a well-defined glacial trough up to 1,000 m deep (Figs. 3 and

4). The trunk canyon is joined by five tributary canyons up to 5.5 km in length (M1-M5, Fig. 5). The main trunk is lined by debris fans and talus cones that, in places, are nearly joined across the valley. There is a prominent 750 m-long by 500 m-wide **roche moutonnée** centrally located in the main trunk; its southwestern

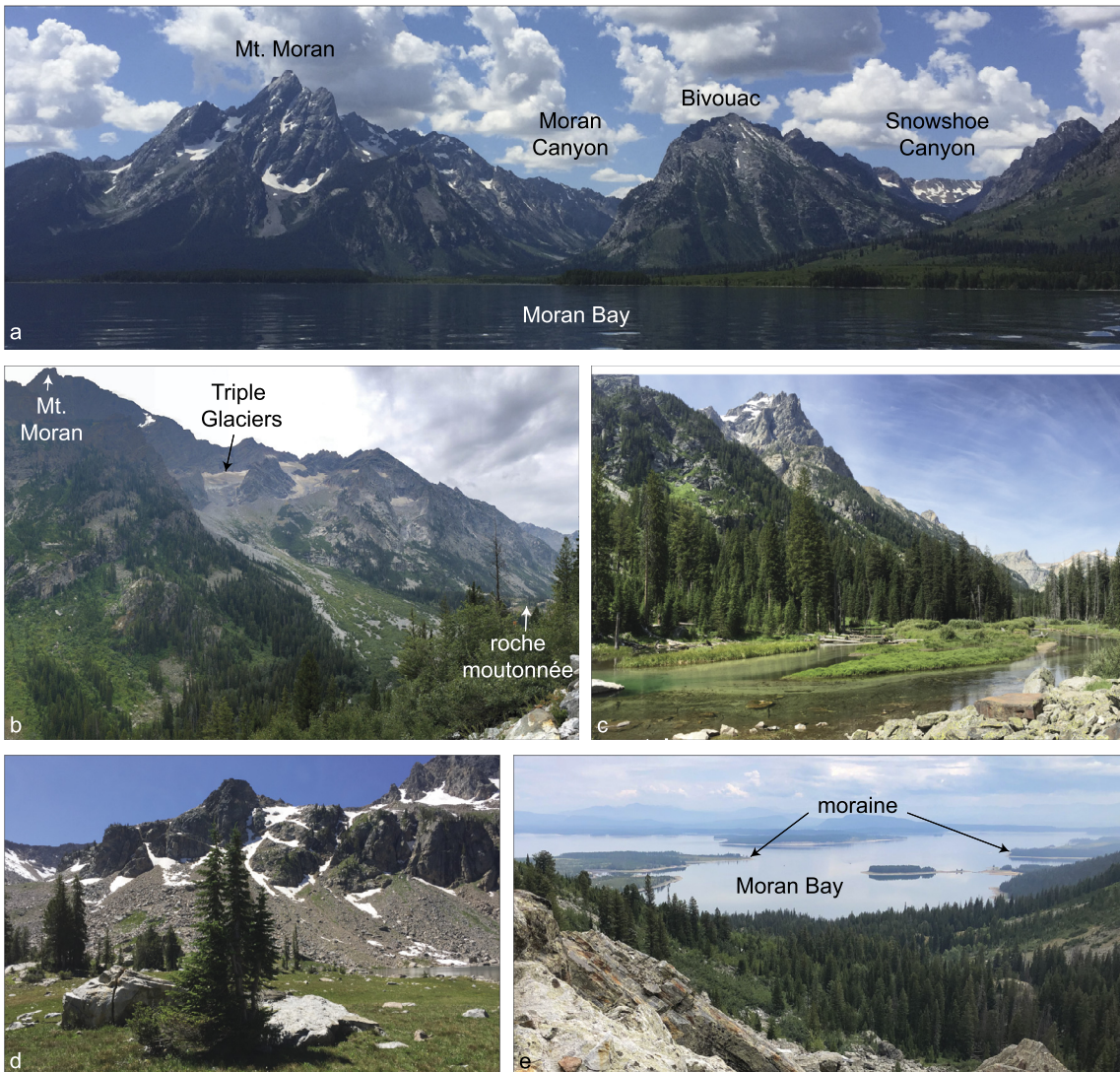


Fig. 4. Examples of landforms in the Teton Range: a) view of Moran and Snowshoe Canyons from Moran Bay, b) view of Mt. Moran, Triple Glaciers, debris fan, talus cones and a roche moutonnée in Moran Canyon, c) alluvium in a glacially-flattened valley, d) talus cones, e) view from Moran Canyon of Moran Bay and the moraine that isolates it from Jackson Lake.

edge aligns with a NW striking dike that crosses the valley (e.g., Love et al., 1992). Upstream of the roche moutonnée, Moran Creek has developed a relatively flat 1.8 km-long by 0.3 km-wide alluvial plain. Downstream, the valley gradient steepens where it descends through knobby bedrock to Moran Bay. The western edge of Moran Bay is defined by the modern Teton fault scarp.

Each Moran Canyon tributary displays a unique subset of landforms, longitudinal profiles, and channel characteristics (Fig. 5). Tributary M1 has a relatively smooth graded profile, with a valley floor lined with glacial drift and a network of gullies. Talus cones and debris fans are less prevalent here and do not extend far into the valley. Tributary M2 is similar to M1, but there is a knickpoint before it joins M1. Here the toe of a debris flow deposit has been eroded to produce an incised bedrock channel >5 m deep. Tributary M3 includes the largest lake in the catchment, Cirque Lake. M3 does not have a well-developed trough shape, and the valley floor is mostly knobby bedrock. The channel that drains the overflow from Cirque Lake flows over bedrock, glacial drift and around the base of talus cones as it drops to join M1. Tributary M4 is dominated by talus cones and debris fans that overlap to form an irregular valley floor with no continuous channel. Where the slope steepens to join the main trunk, the valley floor is lined by

glacial drift incised by a small channel. Tributary M5 drains Triple Glaciers on the northwestern flank of Mt. Moran (elev. 3842 m). Here the largest debris fan in the study area extends down the axis of the valley and across the floor of Moran Canyon (Fig. 4). A channel draining the glacier disappears underground partway down the fan.

The Snowshoe catchment (26.4 km²) is composed of a main trunk with tributary canyons up to 3 km in length and several small glacial basins (S1-S4, Fig. 5). Unlike the graded longitudinal profiles in the Moran catchment, the valleys in Snowshoe have multiple knickpoints, and the surface topography is much rougher (Figs. 3 and 5). The north wall of the main trunk is lined by talus cones and the southern side consists of multiple small glacial basins with moraines, rock glaciers, tarns, talus cones and talus slopes. Snowshoe Canyon is drained by North Moran Creek, which exits the canyon and flows across glacial drift, where it forms a 1.3 km by 0.4 km wide alluvial plain adjacent to Moran Bay.

The longitudinal profile of S1 has four knickpoints before it is joined by S3 and S4. The flat parts of the stepped valley floor are composed of either glacial drift at high elevations or alluvium at lower elevations. The steep portions of each step are composed of bedrock channels. S2 is distinguished by the largest rock glacier

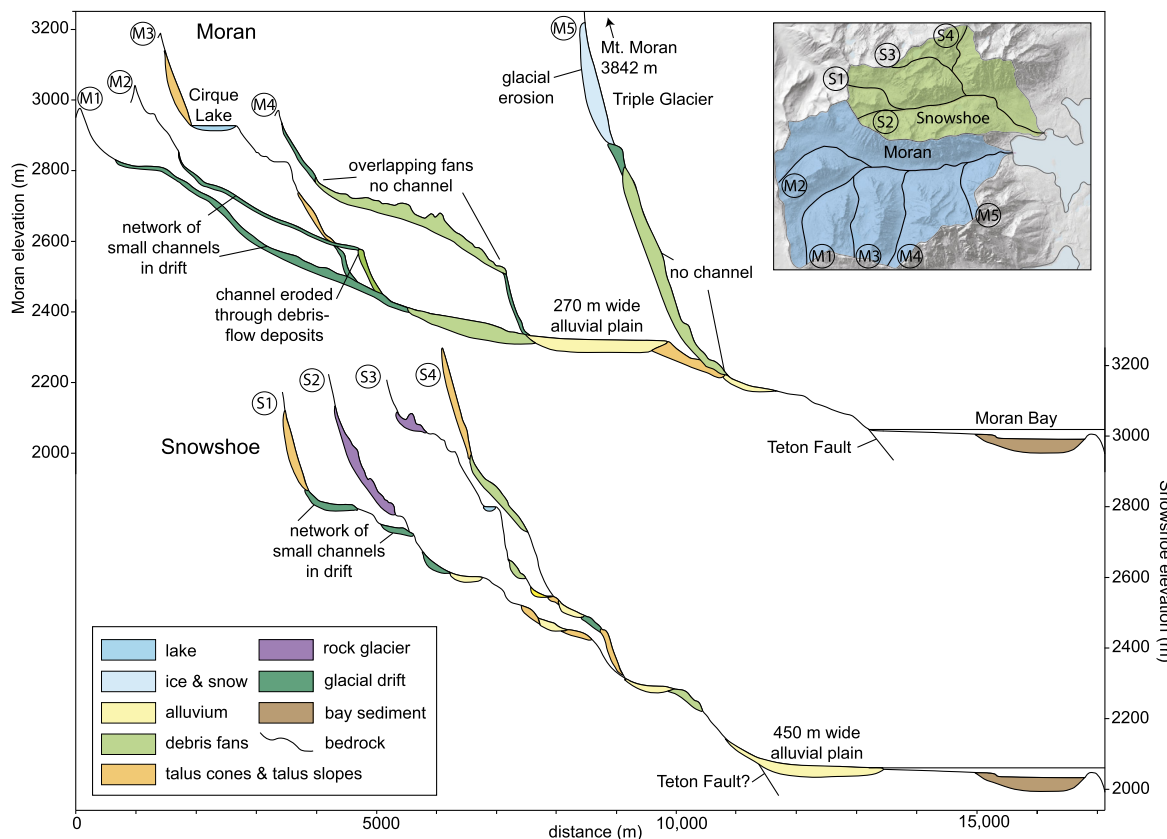


Fig. 5. Stream profiles and geomorphic units along major tributary valleys of the Moran and Snowshoe catchments. Geomorphic units in contact with the valley bottom are shown, but depths are not implied.

(~1.2-km-long) in the catchment. The upper half of S3 is composed of knobby bedrock with several tarns, rock glaciers and drift, and lacks a well-developed channel. Where it is joined by tributary S4, the valley has a trough-shape and a channel bordered by talus cones. In tributary S4 the channel flows between glacial drift and debris fans, and then over bedrock as the valley steepens to join S3.

3.2. Moran Bay seismic reflection profiling

Seismic profile D19, which extends through the midline of Moran Bay and into the main depocenter of Jackson Lake, reveals that the bay is effectively perched above and is isolated from the main depocenter by a bathymetric ridge, essentially trapping the post-glacial sediment derived from the two catchments (Fig. 6). Moran Bay sedimentary packages are separated by three key horizons that are interpreted to reflect major changes in depositional character.

Horizon A, which defines the top of the acoustic basement beneath which there is no internal reflectivity, is an uneven surface with maximum and minimum depths of ~47 m and ~9 m below the modern lake surface, respectively. This surface also defines the top of the bathymetric ridge that separates Moran Bay from the main Jackson Lake depocenter (Fig. 6). Lake bottom gravity cores attempted along the ridge had limited penetration depth and yielded mostly sand and gravel (Table 1). Horizon B4 defines the top of a package of internally stratified yet pervasively deformed sediment that is overlain by an essentially undeformed sediment package. Horizon C3 defines the lake bottom.

Between Horizons A and B4, the pervasively deformed sediment package within which there are four distinctive subunits (Fig. 6c). B1 is the lowermost and is up to 9 m thick, discontinuous, with distorted internal reflectors. B2 is a set of parallel reflectors up to

14 m thick which are deformed by folding. B3 is a 6 m thick package ~20 m below the modern lake surface. B4 is a set of parallel reflectors that onlap B3. All of the reflectors between Horizons A and B are offset along two discontinuities which terminate at Horizon B. Intermediate reflectors between Horizons B4 and C3 appear mostly undeformed and three subunits can be separated (Fig. 6c). C1 lies atop B3, is 1 to 2 m thick and nearly horizontal. C2 is a 7 m-thick stack of two clinoforms ~12 m below the modern lake surface. It extends 450 m from the western edge of the seismic line. C3 is a low amplitude highly continuous package up to 9 m thick that onlaps the clinoforms and is ponded in the center, and the top of which gently slopes to the east. Gravity cores collected from the lake bottom and across Horizon C yield laminated silty and sandy clay with variable amounts of organic matter and muddy sand with charcoal (Fig. 6, Table 1). For the volume estimates discussed below, we consider Horizons A and C to represent the bottom and top, respectively, of the Moran Bay post-glacial sediment package.

3.3. Estimates of sediment volume, post-glacial sediment production, and erosion rates

Monte Carlo simulations yield total post-glacial (post- 14.4 ± 0.8 ka) rock volumes of $169.38 \pm 35.09 (\times 10^{-3} \text{ km}^3)$ for the canyon catchments, a total rock volume in Moran bay of $4.44 \pm 0.90 \times 10^{-3} \text{ km}^3$, and a total post-glacial rock volume of $173.82 \pm 35.99 \times 10^{-3} \text{ km}^3$ (Table 2). These simulated volumes include uncertainties discussed in the methods section. These volume estimates yield a post-glacial sediment production rate of $0.17 \pm 0.02 \text{ mm/yr}$ and an average catchment-wide post-glacial fluvial erosion rate of $0.004 \pm 0.001 \text{ mm/yr}$. Based on these estimates, the Moran Bay sediment volume represents only ~2.6% of the post-

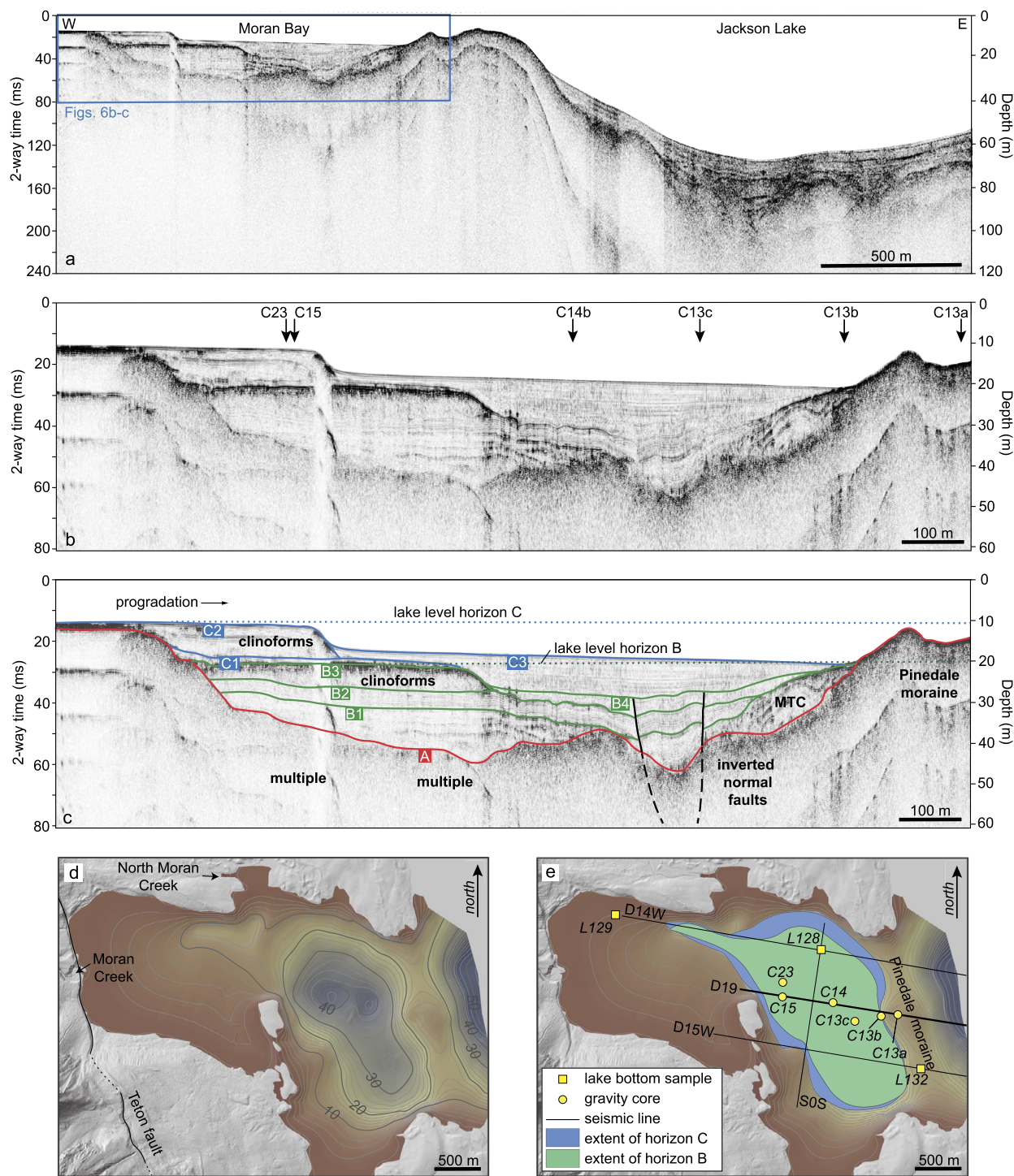


Fig. 6. CHIRP seismic profiles and maps of Moran Bay. a) Seismic profile D19 showing Moran Bay is isolated from the main depocenter of Jackson Lake by a submerged bathymetric ridge. b) Moran Bay seismic profile with locations of lake bottom samples and gravity cores. c) Interpretation of the seismic profile. d) Paleobathymetric map of Moran Bay based on horizon A, the Pinedale moraine. e) Map showing the horizontal extents of horizons B and C, and the locations of seismic lines, short cores and lake bottom samples.

glacial sediment volume stored in Moran and Snowshoe Canyons (Table 2). In an end member scenario where assigned canyon sediment thicknesses were zeroed and the lower estimated volumes based on uncertainty are used, while the Moran Bay sediment column is maximized based on uncertainty (ignoring organic matter, autochthonous carbonate, and biogenic silica); the post-glacial bay sediment volume is only 4.7% of the minimum sediment estimated in the canyons.

4. Discussion

4.1. Moran Bay impoundment timing, geometry, and sedimentation history

Key to making useful comparisons of different stored sediment volumes in the Moran/Snowshoe system is the necessity to demonstrate that the majority of post-glacial sediment exiting the canyons is actually deposited and remains in Moran Bay. Seismic

Table 1

Moran Bay gravity core and lake bottom sample locations and descriptions.

Horizon Sampled	Sample	Sample type	Sample ID	Location	Description
A	C13a	Gravity core	No yield	522794, 4856242	No core, sample of sand and gravel
A	C13b	Gravity core	No yield	522640, 4856234	No core, mud on top of hard surface
A	L132	Lake bottom	JL-GB-132	522987, 4855772	Brown-grey pebbly muddy medium sand with charcoal
C	C13c	Gravity core	JL19-13.5A-1G	522410, 4856188	34 cm silty and sandy clay, massive to discontinuously laminated
C	C14b	Gravity core	JL19-14B-1G	522216, 4856352	34 cm silty and sandy clay, discontinuously laminated
C	C15	Gravity core	JL19-15-1G	521772, 4856401	29 cm grey structureless mud with abundant coarse plant macrophyte fragments
C	C23	Gravity core	JL19-23-1G	521774, 4856529	32 cm silty and sandy clay, discontinuously laminated
C	L128	Lake bottom	JL-GB-128	522112, 4856812	Brown-grey sandy muddy charcoal
Landward of seismic lines	L129	Lake bottom	JL-GB-129	520288, 4857118	Brown-grey muddy sand with charcoal

Table 2Summary of area and sediment volume calculations in Moran Canyon, Snowshoe Canyon and Moran Bay. Volume analysis is based on a combination of the modeled bedrock DEM analysis, sediment production rate of colluvium and assigned thicknesses based on landform observations. Bulk sediment volumes are converted to rock volumes using a Monte Carlo simulation that incorporates a range of porosities for the material, and a $\pm 20\%$ potential error in the bulk volume estimate.

Landform	Bulk volume ($\times 10^{-3}$ km 3)		Total bulk volume ($\times 10^{-3}$ km 3)	Rock volume ($\times 10^{-3}$ km 3)		Post-glacial volume (%)	
	Modeled bedrock DEM area	Outside bedrock DEM area		Including assigned thickness areas	Without assigned thickness areas	Including assigned thickness areas	Without assigned thickness areas
Talus cones & debris fans	81.39 \pm 16.27	84.31 \pm 16.86	165.70 \pm 33.13	127.59 \pm 25.63	127.59 \pm 25.63	73.41	89.22
Talus slopes	5.42 \pm 1.08	17.23 \pm 3.45	22.65 \pm 4.53	17.45 \pm 3.50	4.17 \pm 0.84	10.04	2.92
Alluvium	9.33 \pm 1.87	3.73 \pm 0.75	13.06 \pm 2.62	9.53 \pm 2.36	6.81 \pm 1.69	5.48	4.76
Rock glacier	–	13.54 \pm 2.71	13.54 \pm 2.71	10.56 \pm 2.56	–	6.08	–
Cirque moraine	–	4.91 \pm 0.98	4.91 \pm 0.98	3.83 \pm 0.93	–	2.20	–
Lacustrine	–	0.55 \pm 0.11	0.55 \pm 0.11	0.42 \pm 0.11	–	0.24	–
Total post-glacial sediment in canyons	96.14 \pm 19.22	124.27 \pm 24.86	220.41 \pm 44.08	169.38 \pm 35.09	138.57 \pm 28.16	97.45	96.90
Moran Bay	–	7.40 \pm 1.48	7.40 \pm 1.48	4.44 \pm 0.90	4.44 \pm 0.90	2.55	3.10
Total post-glacial sediment in the system	96.14 \pm 19.22	131.67 \pm 26.34	227.81 \pm 45.56	173.82 \pm 35.99	143.01 \pm 29.06	100.00	100.00
Glacial drift	11.45 \pm 2.29	28.12 \pm 5.62	39.57 \pm 7.91	30.86 \pm 5.19	8.95 \pm 2.18	–	–

imaging along line D19 shows that the Moran Bay sedimentary sequence is separated from the main depocenter of Jackson Lake by a submerged ridge that provides considerable bathymetric relief relative to the adjacent lake floor (Fig. 6), and other lines (D14W, D15W) demonstrate that this ridge is continuous to the north and south. The lack of internal seismic reflectivity in the units below Horizon A, the mapped geometry and location of the ridge, and the coarse, poorly sorted sediment sampled by the limited gravity cores along this feature (Table 1) informs the interpretation that the ridge is a glacial moraine. Additionally, it is positioned in the same location as the terminal moraines that impound Leigh and Jenny Lakes to the south (Fig. 1) and the submerged ridge is connected to the moraine units exposed at the surface (Love et al., 1992), now referred to as Pinedale-3 (Pierce et al., 2018), which partially encloses Moran Bay at present (Figs. 3, 4, and 6). Formation of this terminal moraine ridge likely occurred as the combined result of the Snake River Lobe flowing southward along the range front, essentially limiting the valley migration of the terminal moraine exiting Moran Canyon. Exact glacial stratigraphic relationships remain uncertain, but it is likely that

this ridge/moraine formed during the Pinedale-2 and Pinedale-3 glacial advances (Pierce et al., 2018). Assuming the age of the now-submerged Moran Bay moraine is equivalent to the inner Pinedale-3 moraine of Jenny Lake, this deglacial surface mapped in this study as Horizon A yields an age of 14.4 \pm 0.8 ka (Pierce et al., 2018), which requires that deposits overlying this horizon are post-glacial.

4.2. Sediment production and erosion rate

Glacial processes modify the landscape to produce U-shaped valley walls and flattened and elongated valley profiles (Harbor, 1992). The de-butressing of steep glacial valley walls upon glacial retreat results in unstable slopes of jointed rock. Rock falls and debris flows then produce the talus cones and debris fans that form the majority of sediment in Moran and Snowshoe Canyons. The basin-wide averaged rate of post-glacial sediment production in Moran and Snowshoe Canyons is 0.17 ± 0.02 mm/yr, which assumes that all of the sediment was deposited after the Pinedale glaciation. This denudation rate does not include chemical weath-

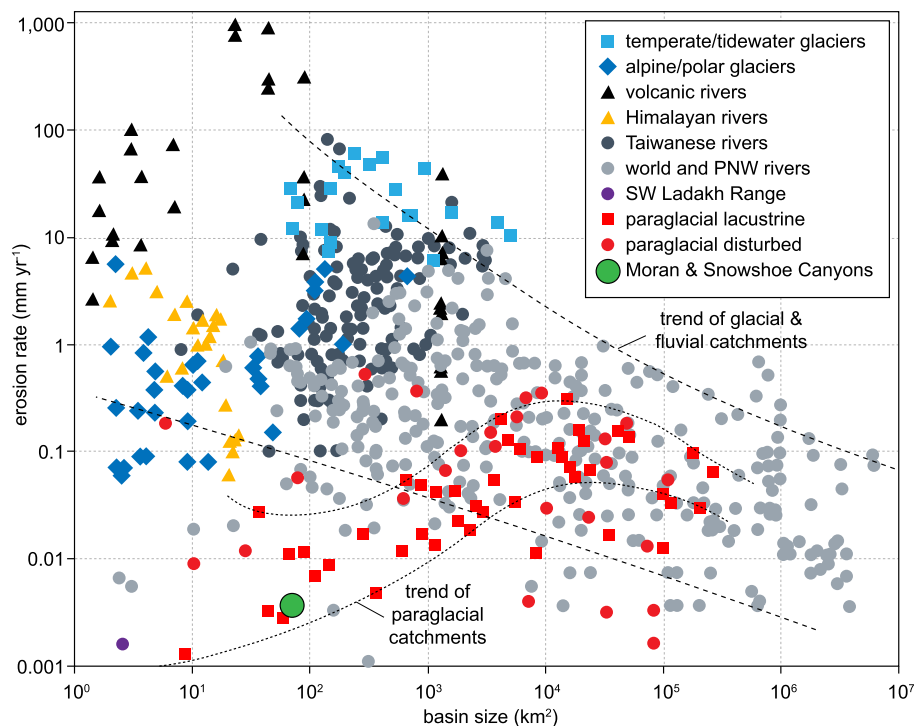


Fig. 7. Erosion rates of fluvial, glacial and paraglacial catchments from Koppes and Montgomery (2009); Church and Slaymaker (1989) and Dietsch et al. (2015). The erosion rate of Moran Bay of 0.004 ± 0.001 mm/yr plots within the typical range for small paraglacial catchments.

ering. The calculated sediment production rate is similar to the long-term denudation rate of 0.14 mm/yr calculated by Brown et al. (2017) using low-temperature thermochronology and the basin-wide post-glacial sediment production rate of 0.13 mm/yr calculated for Garnet Canyon via a combination of hillslope and ridge erosion by Tranel (2015). While the maximum uplift rate along the Teton Fault at Mt. Moran is 0.28 to 0.31 mm/yr (Thigpen et al., 2021), due to the asymmetric uplift of the Teton Range (Brown et al., 2017; Foster et al., 2010), the uplift rate at the heads of the catchments, which are near the center of the range, is approximately 0.14 to 0.16 mm/yr, such that the average uplift of the catchments is roughly 0.21 to 0.23 mm/yr. The similarity of these rates indicates that paraglacial hillslope processes are an essential contributor to the overall erosion rate of the Tetons.

While glacial erosion increased the topographic relief of the valley walls, producing conditions favorable to rockfall, the relief of the valley profile has been reduced, and it is less steep and less concave than fluvial valley profiles (Whipple et al., 1999). This gradient reduction lowers stream power and diminishes sediment transport capacity out of the canyons, producing a system that is transport-limited. While the valleys are apparently steep enough in places for the stream to erode down to bedrock, mobilized sediment may be trapped by subsequent flattened step-like sections below each bedrock reach (Fig. 5). In effect, Teton valleys are almost entirely encompassed in the Periglacial Domain (Hobley et al., 2010; Dietsch et al., 2015), which is characterized by U-shaped valleys dominated by glacial debris, talus, and paraglacial fans, and which lacks trunk streams with the power to transport sediment and incise gorges into their valleys. The lack of transport results in the volume of alluvium stored in the canyons being more than double the volume of sediment that has been transported and deposited into Moran Bay.

In contrast to the rate of sediment production, the catchment-wide post-glacial fluvial erosion rate is just 0.004 ± 0.001 mm/yr, even lower if we constrain autochthonous sediments versus allochthonous sediments from the canyon, pointing to a disconnect

between weathering production and sediment yield, a hallmark of sediment transport in deglaciated terrain (Church and Ryder, 1972; Ballantyne, 2013; Tunnicliffe and Church, 2011). Sources of Moran Bay sediment include glacial drift, periglacial debris, talus cones and debris fans, debris flows that enter the channel, and fluvial and glacial bedrock erosion (Figs. 3, 4, 5). In addition, lake sediments composed of sponges (biogenic silica), ostracods (carbonate), algae (biogenic silica, organic matter) contribute to accumulation patterns in Moran Bay (Rasbold et al., 2022).

Many sediment yield studies have been based on short-term (days to years) observations and thus do not necessarily reflect long-term (10^2 – 10^5 years) rates (Spotila, 2022). It is, however, interesting to compare them with the long-term erosion rate for Moran Bay over the past 14.4 ka. The Moran Bay rate of 0.004 ± 0.001 mm/yr is very low compared to similar-sized fluvial or glacial catchments but is similar to modern rates derived from small deglaciated basins (Fig. 7). In addition, it is notable that modern erosion rates of the larger (>1000 km 2) fluvial and paraglacial basins are similar, whereas in the smaller basins (<1000 km 2), paraglacial erosion rates plot well below the erosion rates of fluvial basins of the same size, suggesting that post-glacial fluvial inefficiency is not uncommon in small deglaciated basins. The difference in erosion rates for smaller catchments could imply that available discharge may play an important role in moving larger caliber debris. Reaches steep enough to erode down to bedrock followed by subsequent trapping of sediment on flattened steps were observed in Moran and Snowshoe Canyons, suggesting that the fluvial system has the discharge to move larger debris during floods but lacks the steepness to evacuate them out of the catchment.

4.3. Landscape, process, and equilibrium

The relative contributions of glacial, fluvial and colluvial processes to an equilibrium state between denudation and rock uplift change over long (multi-glacial cycle) or interglacial timescales. Numerical models suggest that glacial erosion rates can be higher

than rock uplift rates when the topography is adjusting from fluvial to glacial conditions or if there is a shift in climate periodicity (e.g., Pedersen and Egholm, 2013). Once the glacial valley is carved and adjusted to glacial erosion, subsequent glaciers may not need to erode much bedrock to maintain this equilibrium (i.e., match rock uplift rates), but primarily transport the hillslope sediment deposited during the interglacial, and do a little erosion to maintain the valley shape (Herman and Braun, 2008; Leith et al., 2014), thus maintaining a glacial steady state (Deal and Prasicek, 2021). The similarity of the colluvial production rate and the long-term denudation rate in the Tetons indicates that hillslope processes are an essential contributor to the denudation of the Tetons over long timescales. In the Tetons, the larger basins ($>20 \text{ km}^2$) have hosted glaciers capable of keeping pace with rock uplift and maintaining a shallow longitudinal valley profile (Foster et al., 2010). However, since the topography has adjusted to accommodate glaciation, glaciers may not produce substantial primary bedrock erosion along the valley bottoms as they do at higher elevations; thus, the mass efflux from the larger canyons is dominated by interglacial colluvial sediment production and eventual transport during the next glacial advance (Tranel et al., 2011). Hillslope processes, with glacial advances providing sediment transport, may be at least as important for attaining steady state as canyon incision (Brocklehurst and Whipple, 2007).

While glacial and colluvial processes appear to have the capacity to equilibrate with uplift in the Tetons, the capacity of the fluvial system to equilibrate with uplift has been hampered because the valley profile has been flattened by glaciers. In fluvial-dominated landscapes, rivers govern the landscape response by setting local base level and controlling the hillslope angle needed for denudation rates to match rock uplift rates, which drives the channel systems toward graded equilibrium longitudinal profiles (Whipple et al., 2013). If perturbed by a change in a boundary condition, such as a change in base level due to fault slip, the fluvial system will respond by transiently adjusting to a new steady-state. For example, the longitudinal profile of a stream will work to adjust to fault slip through vertical incision and knickpoint migration (e.g. Whipple and Tucker, 1999). In the context of this study, the fluvial system has been “perturbed” by glacial erosion flattening the valley, to which the river system needs to transiently steepen to once again compete with rock uplift. Here, it is evident that the fluvial system is disequilibrated by such a “glacial perturbation”, with interglacial fluvial processes yielding a post-glacial fluvial erosion rate of just $0.004 \pm 0.001 \text{ mm/yr}$, which is far outpaced by the maximum uplift rate of 0.28 to 0.31 mm/yr for the Teton Range. The difference between sediment production in the canyons and sediment yield into the bay, means that $\sim 97\%$ of the canyon sediment cannot be transported until the next glacial advance, or the eventual relaxation of the catchment to a fluvial equilibrium landscape.

For rivers to respond to uplift they must have the right topographic conditions to do so effectively. Clearly, the erosive power of rivers in Moran and Snowshoe Canyons is significantly diminished by a landscape that is equilibrated for glacial (and colluvial) processes. In this paraglacial landscape, streams do not set limits on topography but instead are controlled by the post-glacial topography, thus illustrating the importance of the topographic signature as a boundary condition that governs landscape response to uplift.

4.4. Post-glacial landscape longevity

The time required for a deglaciated valley to re-equilibrate to fluvial conditions is strongly controlled by both precipitation and catchment area (Hobley et al., 2010; Dortch et al., 2011), such that the fluvial system is too sluggish to re-equilibrate during interglacial periods. The time required to develop a classic U-shaped

glacial valley that was previously dominated by fluvial processes has been estimated as $<100 \text{ ka}$ (Harbor, 1992). However, the time required to return to a fluvially equilibrated system is far longer, requiring a minimum of 500 ka (Hobley et al., 2010) which is longer than the typical time interval between periods of ice advance (Tomkin, 2009). The lack of modern-day landscapes that are observed to be in transition from glacial to fluvial process dominance highlights the longevity of glacial landscapes (Spotila, 2022).

It is interesting to consider what the effects of a warming climate and the prolonged absence of glaciers might be on the Teton Range. Assuming footwall uplift continues due to slip on the Teton fault, the absence of major glaciers, and a consistent precipitation rate, the elevation of the Teton Range would be expected to increase until a threshold steepness is reached that yields efficient fluvial incision, perhaps eventually leaving a paleo-glacial “terrace” perched above the rejuvenated fluvial landscape. However, as past glaciers have been responsible for moving accumulated sediment out of the valleys and into the Snake River Valley, thus moving the sediment load across the Teton fault and onto the hanging wall, it is possible that the absence of major glaciers could cause a reduction in the rate of uplift, at least until fluvial processes attain the ability to move mass across the fault. Flattened valley profiles are typical of deglaciated catchments around the world. Future climate change and the loss of glaciers will produce more catchments with rivers lacking the capacity to transport sediment, which can potentially impact not only sediment flux, but uplift rates as well.

5. Conclusions

The Teton Range is an ideal setting to quantify fluvial efficiency in a post-glacial landscape. All canyon-sourced sediment is captured in a lake formed by a glacial moraine, allowing a complete post-glacial sediment budget to be constructed. The sediment budget was constructed using existing LiDAR data and newly acquired seismic profiles through Moran Bay. The flattened valley profiles of these catchments are typical of the Tetons, and of deglaciated catchments of similar size around the world. The catchment-wide sediment production rate of $0.17 \pm 0.02 \text{ mm/yr}$ is close to the average catchment uplift rate and the long-term denudation rate of the Teton Range, illustrating the importance of hillslope processes to the overall denudation of the Tetons. This also implies that once topography is adjusted for glacial erosion, subsequent glaciers mostly transport accumulated sediment and may only need to provide some maintenance erosion of bedrock to maintain this equilibrium.

While the combination of glacial and colluvial processes can keep pace with uplift in the Tetons, the interglacial fluvial system cannot, as evidenced by the fact that only $\sim 2.6\%$ of the total post-glacial sediment volume has been transported to the bay. The fluvial system has been perturbed by glacial erosion flattening the valley profiles, reducing stream power and sediment transport capacity. The post-glacial fluvial erosion rate is just $0.004 \pm 0.001 \text{ mm/yr}$, which is far outpaced by the maximum uplift rate of 0.28 to 0.31 mm/yr for the Teton Range, illustrating that glacially-flattened valley profiles preclude fluvial efficiency.

Rivers require the right topographic conditions to respond to uplift. As the erosive capability of rivers in Moran and Snowshoe Canyons has been diminished by a landscape equilibrated for glacial erosion, the accumulating sediment will remain in the catchments until the next glacial advance, or until continued uplift along the Teton fault steepens the topography to make fluvial processes efficient once again. Thus, glacial topography is demonstrated to be not only a record of climate and tectonic dynamics, but an important boundary condition. It appreciably limits rates of denudation and sediment transport, and therefore the ability of the landscape to respond to uplift.

CRediT authorship contribution statement

Sarah E. Johnson: Conceptualization, Formal analysis, Investigation, Methodology, Project administration, Software, Visualization, Writing – original draft. **Meredith L. Swallom:** Formal analysis, Investigation, Methodology. **Ryan Thigpen:** Conceptualization, Funding acquisition, Investigation, Project administration, Resources, Supervision, Writing – review & editing. **Michael McGlue:** Funding acquisition, Investigation, Project administration, Resources, Writing – review & editing. **Jason M. Dorch:** Conceptualization, Writing – review & editing. **Sean Gallen:** Conceptualization, Writing – review & editing. **Edward Woolery:** Funding acquisition, Investigation. **Kevin M. Yeager:** Resources, Writing – review & editing.

Declaration of competing interest

The authors declare that they have no known competing financial interests or personal relationships that could have appeared to influence the work reported in this paper.

Acknowledgements

This work was supported by a UW-NPS seed grant and NSF-EAR 1932808, the Overcash Field Fund at UK, and UK student research grants. We would also like to acknowledge Cooper Cearly, Ryan Goldsby, Autumn Helfrich, Hillary Johnson, and Giliane Rasbold for their work in the field. Comments from two anonymous reviewers greatly improved an earlier version of this manuscript.

References

- Adams, B.A., Whipple, K.X., Forte, A.M., Heimsath, A.M., Hodges, K.V., 2020. Climate controls on erosion in tectonically active landscapes. *Sci. Adv.* 6 (42), eaaz3166. <https://doi.org/10.1126/sciadv.aaz3166>.
- Ardelean, A.C., Onaca, A., Urdea, P., Sărăşan, A., 2017. Quantifying postglacial sediment storage and denudation rates in a small Alpine catchment of the Făgăraş Mountains (Romania). *Sci. Total Environ.*, 599–600. <https://doi.org/10.1016/j.scitotenv.2017.05.131>. pp. 1756–1767.
- Ballantyne, C.K., 2013. Permafrost and periglacial features | paraglacial geomorphology. In: *Encyclopedia of Quaternary Science*. Elsevier, pp. 553–565.
- Binnie, S.A., Summerfield, M.A., 2013. 7.6 Rates of denudation. In: *Treatise on Geomorphology*. Elsevier, pp. 66–72.
- Brocklehurst, S.H., Whipple, K.X., 2007. Response of glacial landscapes to spatial variations in rock uplift rate. *J. Geophys. Res.* 112 (F2), F02035. <https://doi.org/10.1029/2006JF000667>.
- Brown, S.J., Thigpen, J.R., Spotila, J.A., Krugh, W.C., Tranel, L.M., Orme, D.A., 2017. Onset timing and slip history of the Teton fault, Wyoming: a multidisciplinary reevaluation: timing of onset of the Teton fault. *Tectonics* 36 (11), 2669–2692. <https://doi.org/10.1002/2016TC004462>.
- Church, M., Ryder, J.M., 1972. Paraglacial sedimentation: a consideration of fluvial processes conditioned by glaciation. *Geol. Soc. Am. Bull.* 83 (10), 3059. [https://doi.org/10.1130/0016-7606\(1972\)83\[3059:PSACOF\]2.0.CO;2](https://doi.org/10.1130/0016-7606(1972)83[3059:PSACOF]2.0.CO;2).
- Church, M., Slaymaker, O., 1989. Disequilibrium of Holocene sediment yield in glaciated British Columbia. *Nature* 337.
- Deal, E., Prasicek, G., 2021. The sliding ice incision model: a new approach to understanding glacial landscape evolution. *Geophys. Res. Lett.* 48 (1). <https://doi.org/10.1029/2020GL089263>.
- Dietsch, C., Dorch, J.M., Reynhout, S.A., Owen, L.A., Caffee, M.W., 2015. Very slow erosion rates and landscape preservation across the southwestern slope of the Ladakh range, India. *Earth Surf. Process. Landf.* 40 (3), 389–402. <https://doi.org/10.1002/esp.3640>.
- Dorch, J.M., Owen, L.A., Schoenbohm, L.M., Caffee, M.W., 2011. Asymmetrical erosion and morphological development of the central Ladakh range, northern India. *Geomorphology* 135 (1–2), 167–180. <https://doi.org/10.1016/j.geomorph.2011.08.014>.
- DuRoss, C.B., Gold, R.D., Briggs, R.W., Delano, J.E., Ostendar, D.A., Zellman, M.S., Cholewiński, N., Wittke, S.J., Mahan, S.A., 2019. Holocene earthquake history and slip rate of the southern Teton fault, Wyoming, USA. *GSA Bull.* <https://doi.org/10.1130/B35363.1>.
- Egholm, D.L., Nielsen, S.B., Pedersen, V.K., Lesemann, J.-E., 2009. Glacial effects limiting mountain height. *Nature* 460 (7257), 884–887. <https://doi.org/10.1038/nature08263>.
- Fame, M.L., Owen, L.A., Spotila, J.A., Dorch, J.M., Caffee, M.W., 2018. Tracking paraglacial sediment with cosmogenic 10Be using an example from the northwest Scottish Highlands. *Quat. Sci. Rev.* 182, 20–36. <https://doi.org/10.1016/j.quascirev.2017.12.017>.
- Foster, D., Brocklehurst, S.H., Gawthorpe, R.L., 2010. Glacial-topographic interactions in the Teton Range, Wyoming. *J. Geophys. Res.* 115 (F1). <https://doi.org/10.1029/2008JF001135>.
- Frings, R.M., Schütttrumpf, H., Vollmer, S., 2011. Verification of porosity predictors for fluvial sand-gravel deposits: porosity prediction. *Water Resour. Res.* 47 (7). <https://doi.org/10.1029/2010WR009690>.
- Good, J.E.G., Pierce, K.L., 2016. Interpreting the Landscapes of Grand Teton and Yellowstone National Parks: Recent and Ongoing Geology. *Grand Teton National History*.
- Harbor, J., 1992. Numerical modeling of the development of U-shaped valleys by glacial erosion. *Geol. Soc. Am. Bull.* 12.
- Hauck, C., Böttcher, M., Maurer, H., 2011. A new model for estimating subsurface ice content based on combined electrical and seismic data sets. *Cryosphere* 5 (2), 453–468. <https://doi.org/10.5194/tc-5-453-2011>.
- Herman, F., Braun, J., 2008. Evolution of the glacial landscape of the Southern Alps of New Zealand: insights from a glacial erosion model. *J. Geophys. Res.* 113 (F2), F02009. <https://doi.org/10.1029/2007JF000807>.
- Herman, F., De Doncker, F., Delaney, I., Prasicek, G., Koppes, M., 2021. The impact of glaciers on mountain erosion. *Nat. Rev. Earth Environ.* 2 (6), 422–435. <https://doi.org/10.1038/s43017-021-00165-9>.
- Hobley, D.E.J., Sinclair, H.D., Cowie, P.A., 2010. Processes, rates, and time scales of fluvial response in an ancient postglacial landscape of the northwest Indian Himalaya. *Geol. Soc. Am. Bull.* 122 (9–10), 1569–1584. <https://doi.org/10.1130/B30048.1>.
- Kilfeather, A.A., van der Meer, J.J.M., 2008. Pore size, shape and connectivity in tills and their relationship to deformation processes. *Quat. Sci. Rev.* 27 (3–4), 250–266. <https://doi.org/10.1016/j.quascirev.2006.12.015>.
- Kindinger, J.G., Davis, J.B., Flocks, J.G., 1994. High-resolution single-channel seismic reflection surveys of Orange Lake and other selected sites of North central Florida. Report No. 94–616; Open-File Report. USGS Publications Warehouse.
- Koppes, M.N., Montgomery, D.R., 2009. The relative efficacy of fluvial and glacial erosion over modern to orogenic timescales. *Nat. Geosci.* 2 (9), 644–647. <https://doi.org/10.1038/ngeo616>.
- Korup, O., Montgomery, D.R., 2008. Tibetan Plateau river incision inhibited by glacial stabilization of the Tsangpo gorge. *Nature* 455 (7214), 786–789. <https://doi.org/10.1038/nature07322>.
- Leith, K., Moore, J.R., Amann, F., Loew, S., 2014. Subglacial extensional fracture development and implications for Alpine Valley evolution. *J. Geophys. Res., Earth Surf.* 119 (1), 62–81. <https://doi.org/10.1002/2012JF002691>.
- Leopold, L.B., Wolman, M.G., Miller, J.P., 1964. *Fluvial Processes in Geomorphology*. W.H. Freeman & Co.
- Love, J.D., Reed, J.C., Christiansen, A.C., 1992. *Geologic Map of Grand Teton National Park, Teton County, Wyoming. (Map I-2031) [Map]*. USGS.
- Mitchell, S.G., Montgomery, D.R., 2006. Influence of a glacial buzzsaw on the height and morphology of the cascade range in central Washington state, USA. *Quat. Res.* 65 (1), 96–107. <https://doi.org/10.1016/j.yqres.2005.08.018>.
- Moon, S., Page Chamberlain, C., Blisniuk, K., Levine, N., Rood, D.H., Hillel, G.E., 2011. Climatic control of denudation in the deglaciated landscape of the Washington cascades. *Nat. Geosci.* 4 (7), 469–473. <https://doi.org/10.1038/ngeo1159>.
- Norton, K.P., Abbühl, L.M., Schlunegger, F., 2010. Glacial conditioning as an erosional driving force in the Central Alps. *Geology* 38 (7), 655–658. <https://doi.org/10.1130/G31102.1>.
- Otto, J.-C., Schrott, L., Jobyedoff, M., Dikau, R., 2009. Quantifying sediment storage in a high Alpine valley (Turtmannal, Switzerland). *Earth Surf. Process. Landf.* 34 (13), 1726–1742. <https://doi.org/10.1002/esp.1856>.
- Pedersen, V.K., Egholm, D.L., 2013. Glaciations in response to climate variations preconditioned by evolving topography. *Nature* 493 (7431), 206–210. <https://doi.org/10.1038/nature11786>.
- Pierce, K.L., Licciardi, J.M., Good, J.M., Jaworowski, C., 2018. Pleistocene glaciation of the Jackson Hole Area, Wyoming. Report No. 1835; Professional Paper, p. 68. USGS Publications Warehouse. <http://pubs.usgs.gov/publication/pp1835>.
- Rasbold, G.G., Pinheiro, U., Domingos-Luz, L., Dilworth, J., Thigpen, J.R., Pessenda, L.C.R., McGlue, M.M., 2022. First evidence of an extant freshwater sponge fauna in Jackson lake, Grand Teton national park, Wyoming (USA). *Inland Waters*, 1–33. <https://doi.org/10.1080/20442041.2022.2035190>.
- Sass, O., Wollny, K., 2001. Investigations regarding Alpine talus slopes using ground-penetrating radar (GPR) in the Bavarian Alps, Germany. *Earth Surf. Process. Landf.* 26 (10), 1071–1086. <https://doi.org/10.1002/esp.254>.
- Schrott, L., Hufschmidt, G., Hankammer, M., Hoffmann, T., Dikau, R., 2003. Spatial distribution of sediment storage types and quantification of valley fill deposits in an Alpine basin, Reintal, Bavarian Alps, Germany. *Geomorphology* 55 (1–4), 45–63. [https://doi.org/10.1016/S0169-555X\(03\)00131-4](https://doi.org/10.1016/S0169-555X(03)00131-4).
- Spotila, J.A., 2012. Glacially-influenced tectonic geomorphology: the impact of glacial erosion on topography and orogenic systems. In: *Treatise on Geomorphology*. Elsevier, pp. 671–694.
- Thigpen, R., Brown, S.J., Helfrich, A.L., Hoar, R., McGlue, M., Woolery, E., Guenther, W.R., Swallom, M.L., Dixon, S., Gallen, S., 2021. Removal of the Northern

- Paleo-Teton Range along the Yellowstone hotspot track. *Lithosphere* 2021 (1), 1052819. <https://doi.org/10.2113/2021/1052819>.
- Tomkin, J.H., 2009. Numerically simulating Alpine landscapes: the geomorphologic consequences of incorporating glacial erosion in surface process models. *Geomorphology* 103 (2), 180–188. <https://doi.org/10.1016/j.geomorph.2008.04.021>.
- Tranel, L.M., Spotila, J.A., Binnie, S.A., Freeman, S.P.H.T., 2015. Quantifying variable erosion rates to understand the coupling of surface processes in the Teton Range, Wyoming. *Geomorphology* 228, 409–420. <https://doi.org/10.1016/j.geomorph.2014.08.018>.
- Tranel, L.M., Spotila, J.A., Kowalewski, M.J., Waller, C.M., 2011. Spatial variation of erosion in a small, glaciated basin in the Teton Range, Wyoming, based on detrital apatite (U-Th)/He thermochronology: spatial variation of erosion in a small, glaciated basin in the Teton Range, Wyoming. *Basin Res.* 23 (5), 571–590. <https://doi.org/10.1111/j.1365-2117.2011.00502.x>.
- Tunnicliffe, J.F., Church, M., 2011. Scale variation of post-glacial sediment yield in Chilliwack Valley, British Columbia. *Earth Surf. Process. Landf.* 36 (2), 229–243. <https://doi.org/10.1002/esp.2093>.
- Whipple, K.X., 2009. The influence of climate on the tectonic evolution of mountain belts. *Nat. Geosci.* 2 (2), 97–104. <https://doi.org/10.1038/ngeo413>.
- Whipple, K.X., DiBiase, R.A., Crosby, B.T., 2013. 9.28 Bedrock rivers. In: *Treatise on Geomorphology*. Elsevier, pp. 550–573.
- Whipple, K.X., Kirby, E., Brocklehurst, S.H., 1999. Geomorphic limits to climate-induced increases in topographic relief. *Nature* 401 (6748), 39–43. <https://doi.org/10.1038/43375>.
- Whipple, K.X., Tucker, G.E., 1999. Dynamics of the stream-power river incision model: implications for height limits of mountain ranges, landscape response timescales, and research needs. *J. Geophys. Res., Solid Earth* 104 (B8), 17661–17674. <https://doi.org/10.1029/1999JB900120>.
- Whitlock, C., 1993. Postglacial vegetation and climate of Grand Teton and Southern Yellowstone national parks. *Ecol. Monogr.* 63 (2), 27.
- Zhu, Y., Dortch, J.M., Massey, M.A., Haneberg, W.C., Curl, D., 2021. An intelligent swath tool to characterize complex topographic features: theory and application in the Teton Range, Licking River, and Olympus Mons. *Geomorphology* 387, 107778. <https://doi.org/10.1016/j.geomorph.2021.107778>.